Journal of Catalysis 285 (2012) 10–18

Contents lists available at SciVerse ScienceDirect

Journal of Catalysis

journal homepage: www.elsevier.com/locate/jcat

A designed organic–zeolite hybrid acid–base catalyst

Andrew C. Brooks [a], Liam France [b], Cecile Gayot [b], Jerry Pui Ho Li [b,c], Ryan Sault [c], Andrew Stafford [c], John D. Wallis [a], Michael Stockenhuber [b,c,*]

[a] Natural Science Research Centre, School of Science and Technology, Nottingham Trent University, Clifton Lane, Nottingham NG11 8NS, UK
[b] The Catalysis and Nanoscience Laboratory, School of Science and Technology, Nottingham Trent University, Clifton Lane, Nottingham NG11 8NS, UK
[c] Catalysis Research Laboratory, Priority Research Centre for Energy, Chemical Engineering, School of Engineering, The University of Newcastle, Callaghan Campus, NSW 2308, Australia

ARTICLE INFO

Article history:
Received 25 June 2011
Revised 31 August 2011
Accepted 4 September 2011
Available online 26 October 2011

Keywords:
Base zeolite
Organic–inorganic hybrid
In situ IR spectroscopy
Knoevenagel condensation
High thermal stability

ABSTRACT

An organic–zeolite hybrid catalyst was synthesised via solid-state impregnation of the zeolite with an amount of melamine corresponding to 20 mol% of the aluminium content. A high density of basic sites is formed in the zeolite. From infrared spectroscopy and TGA measurements we infer that melaminium cations are formed in the zeolite which are highly thermally stable. IR spectroscopic and TGA measurements showed the presence of melaminium after pre-treatment in vacuum at 450 °C. The catalyst exhibited activity in the Knoevenagel condensation reaction between benzaldehyde and ethyl cyanoacetate which is suggested to be promoted by the presence of acid and base sites. The catalyst activity was compared with other known base catalysts including hydrotalcites and magnesium oxide on alumina support.

1. Introduction

Base catalysed reactions are an important fundamental reaction type in modern organic synthesis. Classic base catalysts are NaOH, KOH, alkali metal (mainly sodium) alcoholates or LDA (lithium diisopropylamide). The catalysts mentioned are all used as homogeneous catalysts, with the usual difficulties of separation, waste disposal and regeneration. Compared to the broad application of acidic zeolites as solid catalysts in chemical processing technology, there has been much less attention paid to basic microporous and mesoporous materials, despite the considerable potential for use in a number of industrially important reactions including aldol additions, condensations and transesterification reactions [1]. Out of all industrial applications of solid acid and base catalysts, only 8% of the processes utilise solid base catalysts, with none of them being basic zeolite catalysts [2]. It is possible to create basic zeolite catalysts by impregnation and ion exchange of alkali metal salts. The basicity of these materials can be tailored by variation of counterion [3] and also aluminium content. These zeolites, however, possess base sites of comparably low strength which limits their applicability to organic synthesis, though the base sites are expected to be more resistant to poisoning from water or carbon dioxide. Alkali metals, metal azides and oxides have also been introduced and stabilised in zeolites. They showed significant basicity [4,5] but exhibited limited stability, site accessibility, diffusion limitation and coking.

There is thus an incentive to develop active and selective heterogeneous catalysts for a number of base-catalysed reactions. Despite some success in the development of heterogeneous base catalysts, such as hydrotalcites [6], MgO [7], alkaline-exchanged zeolites [8], alumina [9] and mesoporous materials [10], the variety and success are still limited. Hydrotalcites, MgO, zeolites and basic alumina exhibit basicity which is related to the bonding and charges on the framework and extra framework oxygen atoms. Organic–inorganic hybrid catalysts have also been reported [11] and though are found to be less strongly basic than the corresponding free organic molecules. Base catalysts can also be created by the introduction of nitrogen-containing groups [12], by first covalently bonding trimethoxysilyl-propyl-*N*,*N*,*N*-trimethylammonium chloride ($SiNR_4Cl$) to the silanol groups of the solid catalyst, before reacting with the organic bases of interest. Using a diamino-functionalised mesoporous silica, Choudary et al. [13] showed how a Knoevenagel condensation between 3,4,5-trimethoxybenzaldehyde and malononitrile took place on a base-modified surface. Due to its open structure, zeolite beta was shown to exhibit excellent rates and diffusion properties for a number of acid-catalysed reactions. Its use as a base catalyst, however, was only recently shown. Some success in producing a basic zeolite beta catalysts was reported by Ernst et al. who used a nitridation method [14]. It was found that such catalysts are active for the Knoevenagel condensation reaction between benzaldehyde and malononitrile and

* Corresponding author at: Catalysis Research Laboratory, Priority Research Centre for Energy, Chemical Engineering, School of Engineering, The University of Newcastle, Callaghan Campus, NSW 2308, Australia.
E-mail address: michael.stockenhuber@newcastle.edu.au (M. Stockenhuber).

0021-9517/$ - see front matter Crown Copyright © 2011 Published by Elsevier Inc. All rights reserved.
doi:10.1016/j.jcat.2011.09.004

that there is a correlation between the degree of benzaldehyde conversion and the amount of nitridation of the zeolite beta catalyst [14]. To overcome diffusional limitations observed in zeolites, mesoporous materials have been tested in condensation reactions with varying success. Recently, zeolites with high mesoporosity have been synthesised and tested for condensation reactions [15,16].

Corma et al. [17] suggest that by changing the chemical composition and activation conditions of the base catalyst, it is possible to have predominantly Lewis or Brønsted base catalysts within a large range of well-defined basicities. Catalysts that contain mild acid–base pairs, such as those that exist in amorphous aluminophosphates (ALPO), have been shown to achieve high selectivity in Knoevenagel condensation of heptanal and benzaldehyde.

The Knoevenagel condensation reaction between ethyl cyanoacetate and benzaldehyde has long been recognised as a relatively simple test for the effectiveness of heterogeneous basic catalysis. Ethyl cyanoacetate has two highly acidic protons in the α position to the nitrile ($pK_a = 9$) [18]. Thus, catalysts of relatively low base strength can be used for the reaction, such as lithium, sodium, potassium and caesium *X* and *Y* type zeolites [19].

In this communication, we report for the first time the modification of a microporous zeolite beta with melamine to form an inorganic–organic hybrid catalyst. Melamine is an organic molecule of medium basicity ($pK_a = 5$) but also possesses high thermal stability [20,21]. This allows for higher activation temperatures. Of interest is the mechanism by which the conversion takes place. We have deliberately chosen the open structure of zeolite beta, whose open pores have a sufficient pore diameter (average mesopore distribution of 1.5–2.0 nm) [22–24] for the best chance of deposition of our base which has a kinetic diameter of 0.62 nm [25]. The presence of micropores allows for good shape selectivity, while the open pore structure is allowing for good interaction with reactants. Our synthesis method for the catalyst is also comparatively simple, compared with other modification methods, as it requires considerably less time and milder conditions. The addition of melamine to the zeolite provides additional base sites to produce acid–base pairs. We also compare the catalytic activity observed in the Knoevenagel condensation of benzaldehyde with ethyl cyanoacetate using this newly developed material, with two other known solid base catalysts, hydrotalcite and MgO/Al_2O_3.

2. Experimental

2.1. Catalyst preparation

2.1.1. Melamine zeolite catalyst, "mel-20-beta and mel-100-beta"

The melamine zeolite catalyst was prepared by thoroughly grinding melamine (99% SigmaAldrich) with an ammonium exchanged zeolite beta (Zeolyst, Si/Al = 12.5, NH_4-beta) in a ball mill for 24 h. The amount of melamine added to the zeolite beta is equivalent to 20 mol% or 100 mol% of the aluminium present in zeolite beta. Catalysts were named mel-20-beta and mel-100-beta, respectively. The rationale to prepare differently loaded catalysts was to produce a purely basic catalyst (mel-100-beta) and a catalyst that contains acid and base sites (mel-20-beta). The mixture was transferred into a quartz calcination boat and heated under a nitrogen atmosphere to 300 °C. The sample was kept at 300 °C for 24 h.

2.1.2. Acid catalyst

Zeolite H-beta was used as an acid catalyst. This form of the catalyst was made by calcining ammonium exchanged zeolite beta (Zeolyst, Si/Al = 12.5, h-beta) at 480 °C for 5 h. Upon reaction, the catalyst was activated by transferring it into a quartz calcination boat and heated under a nitrogen atmosphere to 300 °C. The sample was kept at 300 °C for 24 h.

2.1.3. Hydrotalcite catalyst

Hydrotalcite with an Mg/Al ratio of 2 was prepared via co-precipitation [6]. Two aqueous solutions were prepared, one 70 ml containing 0.35 mol NaOH and 0.09 mol Na_2CO_3 (Aldrich reagentplus ⩾98%), and the other 45 ml of 0.1 mol $Mg(NO_3)_2{\cdot}6H_2O$ (Aldrich ⩾98%) and 0.05 mol $Al(NO_3)_3{\cdot}9H_2O$ (Aldrich ⩾98%). These solutions were slowly added together over one hour under vigorous stirring. The resulting white suspension was heated to 60 °C and continuously stirred for 24 h. The precipitate was then separated using a vacuum filter and washed extensively with distilled water. The sample was then dried at 132 °C for 20 h.

The hydrotalcite catalyst was activated by placing the material in a controlled atmosphere furnace and heated under nitrogen at 5 °C/min to 450 °C for a period of 8 h. It was then left to cool to room temperature. The hydrotalcite was subsequently rehydrated by suspending it in decarbonised water under nitrogen atmosphere for 1 h. The sample was filtered under nitrogen atmosphere and washed thoroughly with decarbonised water and dried in nitrogen flow at 25 °C.

2.1.4. MgO/Al_2O_3 catalyst

MgO/Al_2O_3 was prepared by grinding MgO (Aldrich ⩾98%) and Al_2O_3 (Aldrich ⩾99%) together in a 1:1 M ratio using a mortar and pestle. A small amount of distilled water was added and mixed to form a thick slurry. The sample was then dried at 132 °C for 12 h. After drying, the sample was crushed into a powder and heated in a controlled nitrogen atmosphere furnace to 200 °C and held there for 8 h. The heating rate from room temperature to 200 °C was 5 °C/min.

2.2. Catalytic experimental setup

Prior to reaction, the sample was activated under a nitrogen atmosphere at 450 °C for 1 h, cooled to 77 °C and transferred into a 100 mL glass reactor, which was purged with dry nitrogen. To minimise water adsorption, the catalyst was transferred hot into the vessel. The reaction was performed in the liquid phase at 80 °C under a nitrogen atmosphere, under solventless conditions using an excess of benzaldehyde. The 100-mL glass reactor contained 0.2 mol benzaldehyde (Aldrich reagentplus ⩾99%), 0.117 mol ethyl cyanoacetate (Aldrich ⩾98%), 0.054 mol toluene (Aldrich reagentplus 99%) and typically 300 mg of catalyst. The toluene was added as an internal standard.

The reaction components were quantified using gas chromatography (GC). Two GCs were used for the analysis. The first one was a Shimadzu GC8A equipped with a 3-m-long stainless-steel, 10% OV-17 liquid-phase WHP-supported column. Separation was carried out using a temperature program with the range set at 80–350 °C. The reaction samples were analysed using gas chromatography (GC). The second instrument used for the analysis was a Shimadzu GC-2010 equipped with a 30-m fused silica Rtx®-5 column with a 5% diphenyl/95% dimethyl polysiloxane stationary phase equipped with an FID detector.

Small samples were taken from the reaction vessel at regular intervals over a period of 24 h. Samples were then injected into the GC for analysis. Separation was carried out using a temperature program with the range set at 353–623 K using a ramp rate of 16 K/min, with the carrier gas set to 2 ml/min, on a 100:1 split setting. The final temperature was held for 10 min. Toluene was used as an internal standard, and product and reactants were calibrated using standards. The error on the conversions and yields was found to be ±1% absolute.

Scheme 1. The Knoevenagel condensation between benzaldehyde and ethyl cyanoacetate.

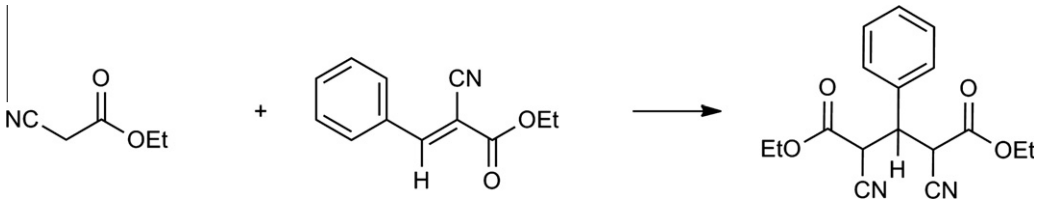

Scheme 2. The Michael addition of ethyl cyanoacetate to ethyl *trans*-α-cyanocinnamate.

2.3. Characterisation

Gravimetric analysis was conducted using a thermal gravimetric analyser (TGA) from Setaram®, model Setsysev™ 1200. The zeolite sample was heated inside the TGA chamber under an inert nitrogen atmosphere. Mass changes were observed as a function of temperature. The surface area and micropore volume of some catalysts were measured by nitrogen adsorption at 77 K using Gemini 11 2370 surface area analyser. Fourier transform infrared spectroscopy (FTIR) was undertaken using an ATI Research Series 1 FTIR Spectrometer. The catalyst was compressed into a disc using a pellet press, activated at 450 °C and then left to cool to 50 °C. Details of the *in situ* experimental setup can be found elsewhere [26].

3. Results and discussion

Scheme 1 shows the reaction equation for the Knoevenagel condensation of benzaldehyde with ethyl cyanoacetate to form ethyl *trans*-α-cyanocinnamate. The reaction often is carried out in DMSO as a solvent, mainly to reduce the undesired consecutive Michael addition side reaction illustrated in Scheme 2. However, over our selective solid-state catalyst (mel-20-beta), the reaction can be performed under solventless conditions without the complication of solvent recovery and no formation of Michael by-product. For cation-exchanged zeolites, the reactivity for the Knoevenagel condensation reaction tends to increase with cation size [27] and aluminium content of the zeolite. Generally, these two parameters are associated with basic strength of the catalyst [16,28]. Catalytic activity was shown to exhibit a complicated pattern with activity maxima dependent on basic site content, strength and crystallinity of the framework and accessibility of the sites in a number of basic catalysts [29]. For example, Cs exchanged SBA-15 which is a highly basic material showed less activity for the condensation reaction than framework nitride zeotypes which are expected to exhibit lower basic strength. Thus, it appears that intermediate basicity is beneficial for the activity of the catalyst. Furthermore, the condensation reaction occurs over sites with moderate basicity, and lower basicity often decreases deactivation. We have thus chosen a relatively weak base (melamine $pK_a = 5$) as our modifier for the zeolite. Melamine can react with the zeolitic acid sites, thereby directly anchoring it to the microporous zeolite beta pore surface by electrostatic interaction and hydrogen bonding. The other nitrogen atoms are then able to form the basic site for the catalytic reaction. The possible bonding between the melamine and the zeolite can be envisaged as indicated in Scheme 3. There is overwhelming evidence from the Cambridge Structural Database [30] that melamine is preferentially protonated on a ring nitrogen atom as shown in over 65 structures of its monocation salts such as its chloride, sulphate and dimesylamide salts [31–33]. Indeed, there are cases where a dication is formed on protonation and both the protons are located on ring nitrogen atoms, as in its bis(trifluoroacetate), sulphate and bis(perchlorate salts) [34–36].

3.1. Characterisation

3.1.1. TGA analysis

Fig. 1 shows TGA analysis of the NH_4-beta zeolite together with the differential TGA (DTGA). The findings are summarised in Table 1. Differential TGA analysis shows that at least two distinct steps can be observed, one centred at 130 °C with a corresponding 4.5% weight loss and one broad maximum at 390 °C with a corresponding weight loss of 2.65% up to 510 °C. The peak at 130 °C can be attributed to desorption of weakly adsorbed water [37], whereas the temperature range of the second weight loss 300–500 °C suggests removal of ammonia from the ammonium form of the zeolite. The weight loss is slightly higher than what would be expected under the assumption of a 1:1 ratio between tetrahedral aluminium and the ammonium cation (1.23 mmol g^{-1}).

Fig. 2 shows the TGA and DTGA curves for the melamine exchanged zeolite (mel-20-beta). Again peaks at lower and higher temperatures were observed in the differential TGA. The low temperature peak (89 °C) is at a slightly lower temperature than the corresponding peak of the NH_4-beta zeolite but the position of the high temperature weight loss (395 °C) is similar. The steps in the TGA curves are significantly more distinct compared with the NH_4-beta zeolite. The amount of weight lost at higher temperatures, attributed to decomposition of ammonium to ammonia, is

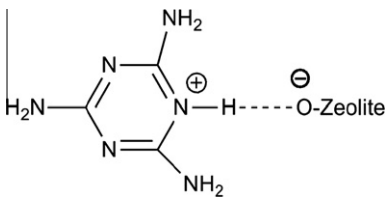

Scheme 3. Structure of the active site.

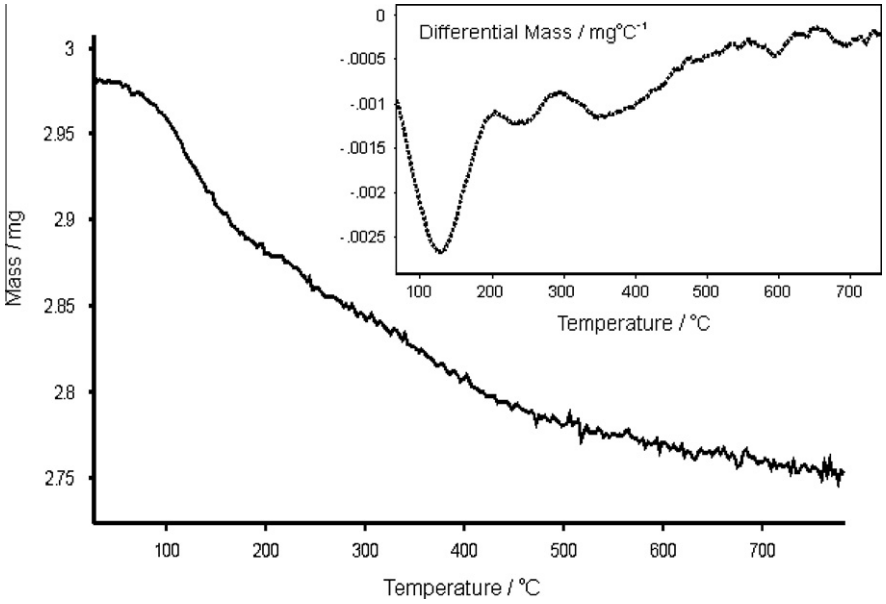

Fig. 1. TGA plot of sample mass (mg) vs temperature (°C), for the NH_4-beta zeolite catalyst.

very similar for mel-20-beta and NH_4-beta zeolites. The similar weight loss suggests that the ammonium ions are still present in the modified catalyst before heat treatment. The high temperature weight loss we observe for both catalysts is higher than would be expected for the aluminium content of the zeolite. Similar behaviour has been found for other zeolites [38]. The main difference between mel-20-beta zeolite catalyst and NH_4-beta zeolite is a less sharp decomposition peak for the NH_4-beta zeolite compared with mel-20-beta zeolite. Although the desorption is occurring over a wider temperature range and is less distinct, the overall weight loss is the same for the two different materials. Broadening of the peak can be explained by a broader energy distribution of the desorption enthalpy. It is expected that the melamine is adsorbing on the stronger sites, consistent with a reduced weight loss at a higher temperature. We can also assume that the ammonium ions are still present after grinding the catalyst with the melamine. It is thus likely that the NH_4^+ cation forms an adduct with the bound melamine. The temperature treatment is suggested to desorb the NH_3 and result in protonation of the melamine to form the cation observed by IR spectroscopy. As evidenced by TGA analysis, thermal decomposition of melamine or melaminium does not take place when the melamine is anchored in the zeolite (since the weight loss we observe is too small). Decomposition of melamine is reported to begin at 500 °C [20]. The absence of significant weight changes at temperatures higher 500 °C suggests stabilisation of the melamine in the zeolite. The weight loss at 395 °C and infrared spectroscopy (see below) are consistent with the presence of a melaminium cation which is expected to exhibit significantly higher stability than the melamine.

Table 1
Adsorption properties of zeolite NH_4-beta and mel-20-beta. Please see text for discussion of ammonia desorption.

Zeolite catalyst	NH_3 loss at temperatures >300 °C ($mmog^{-1}$)	Micropore volume ($cm^3\ g^{-1}$)	Langmuir surface area ($m^2\ g^{-1}$)	External surface area ($m^2\ g^{-1}$)
NH_4-beta	1.86	0.160	731	185
mel-20-beta	1.90	0.127	606	163

3.1.2. In situ FTIR spectroscopy

Fig. 3 shows the *in situ* FTIR spectra of the parent H-beta zeolite and the mel-20-beta catalyst. For the parent H-beta zeolite, bands were seen at 3745, 3609, 1992, 1875, 1713 and 1675 cm^{-1}. The band at 3745 and 3609 cm^{-1} corresponds to stretching vibrations of terminal silanols and bridging hydroxyl groups, respectively. The 1986 and 1872 cm^{-1} bands correspond to overtones of the Si–O stretching bond vibrations [39].

Bands at 3742, 3606, 3378, 3241, 1994, 1870, 1555, 1479 and 1425 cm^{-1} were observed for the activated mel-20-beta sample as well as bands with a central peak at approximately 2240 cm^{-1} (shoulders at 2306, 2239 and 2279 cm^{-1}). The bands in the 3742 and 3606 cm^{-1} region originate from the hydroxyl species of the zeolite framework, associated with terminal O–H groups, and bridging hydroxyls, respectively. This is supported by other FTIR studies reported in literature [14,40,41]. It should be pointed out also that the band at 3606 cm^{-1} when compared with the parent zeolite (the H-beta zeolite) appears to have undergone a red shift, indicating that some interaction has occurred with the bridging hydroxyls present in the zeolite. We observed bands between 1994 cm^{-1} and 1870 cm^{-1} that are also observed in the parent zeolite. These bands are attributed to the overtone bands of the Si–O stretching vibrations reported previously [39]. The bands have been used to normalise for wafer thickness as outlined in [42].

Bands in the 3378 and 3241 cm^{-1} region are attributed to NH stretching vibrations of the side chain primary amines of the melamine, similar to other melamine-derived compounds [43]. The existence of these vibrations shows that the side chain amines in the melamine molecule have not bonded with the zeolite surface.

Observed bands at 1655 cm^{-1}, 1557 cm^{-1} and 1520 cm^{-1} associated with the ring structure of the melamine species were also observed on the mel-20-beta catalyst. 1635 cm^{-1}, 1550 cm^{-1} and 1520 cm^{-1} bands are attributed to the C–N stretching vibrations of the ring nitrogens. The band at 1635 cm^{-1} is attributed to the stretching modes of the aromatic C–N bonds from the ring. Bands in the range of 2240 cm^{-1} can be attributed to vibrations of the amine cation, which are N–H stretching and overtones or combination bands in Fermi resonance. The position of the band at lower wavenumbers suggests that the melamine binds as an amine salt [44]. The IR absorptions are quite unique because only a few

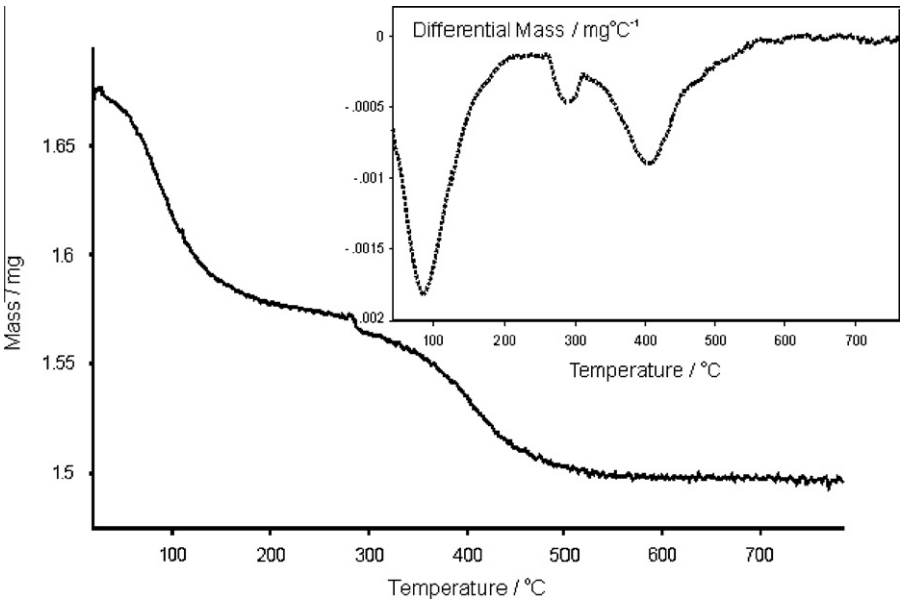

Fig. 2. TGA plot of sample mass (mg) vs temperature (°C), for the mel-20-beta zeolite catalyst.

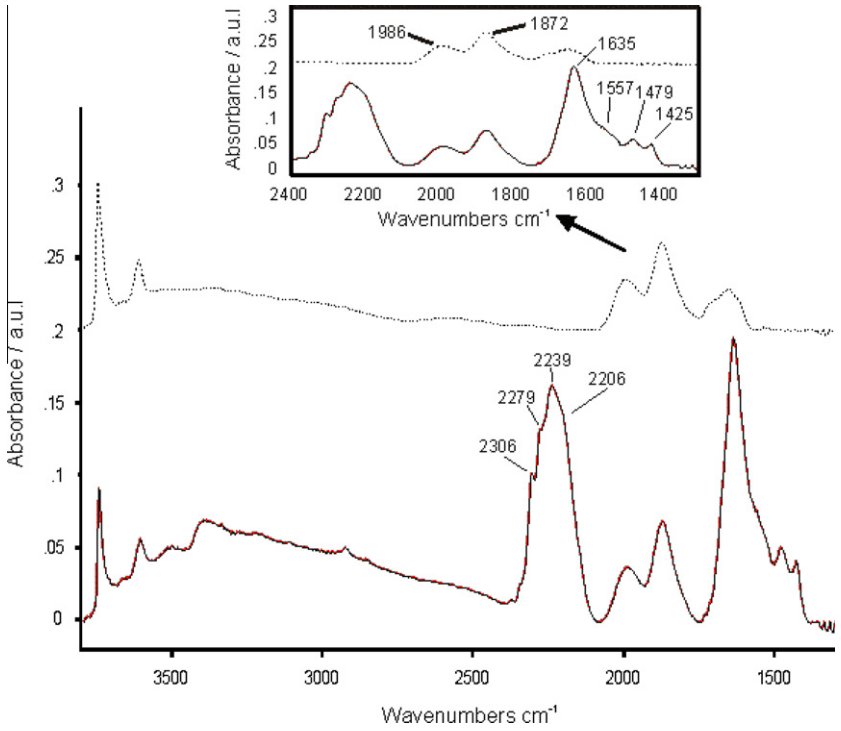

Fig. 3. FTIR spectra comparing H-beta and mel-20-beta zeolite catalysts. Both samples were activated in vacuum ($<10^{-7}$ mbar) at 450 °C.

compounds absorb IR in this region. The NH^+ stretching frequency is a little lower than was observed for halogen salts of amines but is known to depend on the type of counterion. The frequency was found to increase progressively from Cl^- to Br^- and to I^- and was suggested to be associated with hydrogen-bonding interaction with the counteranion [44,45]. Estimation of the partial charge on the cation depending on the type of anion (I^-, Br^-, Cl^- and I^-) using a Sanderson electronegativity model suggests an increase in the cation partial charge on the nitrogen in the amine and corresponding decrease in the frequency. The partial charge on a NH_4^+ cation bonded to the beta zeolite is estimated at 0.17, whereas for NH_4I, it is 0.155. This suggests a decrease in the NH^+ frequency in the melaminium cation due to the zeolite "anion", which is what we observe by comparison with the literature. A paper on the details of the interaction between melamine and the zeolite is in preparation.

Bands at 1479 cm^{-1} and 1425 cm^{-1} are associated with the positively charged amine deformation vibrations from the melamine. The bands show evidence of N–H bending mode and two N–H stretching modes, respectively [46], indicating that a bond between the zeolite and the amine cation from melamine has been formed.

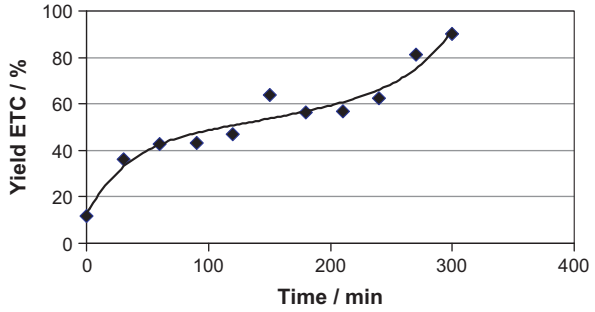

Fig. 4. Percentage yield (ethyl *trans*-α-cyanocinnamate) as a function of time over the mel-20-beta zeolite catalyst.

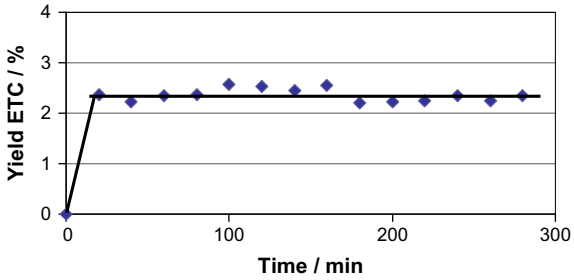

Fig. 5. Percentage yield product (ethyl *trans*-α-cyanocinnamate) using the acid catalyst H-beta zeolite as a function of time.

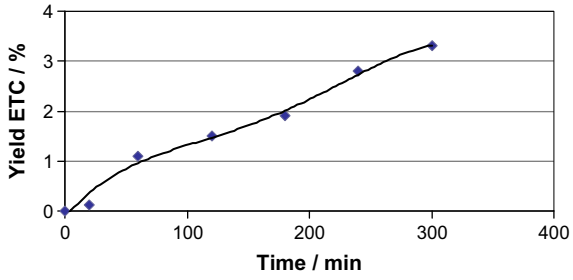

Fig. 6. Percentage yield product (ethyl *trans*-α-cyanocinnamate) without catalyst as a function of time.

Table 2
Product % conversion over 24 h of ethyl cyanoacetate and the respective rates where applicable.

Zeolite catalyst	Product conversion after 24 h (%)	Initial rate (mol/g/min)
mel-20-beta	93.0	0.0015
mel-100-beta	18.0	0.0005
H-beta	13.8	0.0008
Uncatalysed	3.5[a]	–

[a] Michael addition product.

The preparation procedure involves grinding of melamine with the NH_4-beta zeolite and then heating to 450 °C in the infrared spectrometer. It has been suggested that melamine begins to decompose thermally at 500 °C and can form extended condensation products [20]. The formation of these products is expected to be hindered in the zeolite pores. We also observe the characteristic melaminium cation bands after pretreatment at 450 °C, resulting in stabilisation through formation of melaminium cations.

3.2. Catalytic activity of zeolite catalysts

Fig. 4 shows the percentage yield of ethyl *trans*-α-cyanocinnamate based on ethyl cyanoacetate against time for the mel-20-beta zeolite catalyst. No by-product was observed. The initial rates and final conversions over the various catalysts are given in Table 2. It is important to note that we observed significantly lower conversion and rate over mel-100-beta than over mel-20-beta. This suggests changes in the site type and/or mechanism as outlined below. A change in the micropore volume upon modification was observed (Table 1); thus, changes in accessibility variation of the sites in mel-20-beta and mel-100 beta cannot be ruled out. The final conversion at 24 h of ethyl *trans*-α-cyanocinnamate over mel-20-beta was observed to be 93%. The reaction observed using H-beta zeolite catalyst produced a conversion of 13.8% (Fig. 5), with minimal Michael addition product observed, due to the steric hindrance induced from the zeolite pores. The acidic nature of the catalyst, however, makes the formation of the desired product difficult. Similar, we observed 18% conversion over the more basic zeolite mel-100-bea. Thus, the intermediate basicity of zeolite mel-20-beta appears to favour the reaction to the desired product. A conversion of 3.5% after 5 h (Fig. 6) was observed for the uncatalysed reaction with significant formation of the Michael product.

The acid-catalysed reaction was found to exhibit a significantly lower initial rate than our base-catalysed reaction, namely 0.0008 and 0.0015 mol g^{-1} min^{-1}, respectively. Final conversion after 22 h was 11.7% and some benzoic acid formation has been observed as well. Some ethyl *trans*-α-cyanocinnamate as well as some benzoic acid was formed even without the presence of a catalyst.

Our results obtained for the mel-20-beta zeolite are comparable to a report by Zhang et al. [47] whose study involved the grafting of amino groups onto zeolite *X* variants. They observed a 55% conversion over 50 min, indicating that the amino groups were key to catalysing the reaction. Our values compare very well with a recently reported system, layered PLS-1 [48], which exhibited similar end conversions at 70 °C. After 30 min, 80% conversion was observed in toluene. The initial rate based on the data given was 1.3×10^{-3} mol min^{-1} g^{-1}. As can be observed from the above data, over the mel-20-beta zeolite catalyst, no other reactions are observed and the rate of reaction is significantly enhanced compared with the other materials. Scheme 4 shows the mechanism for the acid catalysed condensation reaction. In Scheme 5, the base-catalysed Knoevenagel condensation is shown, which is probably operating over the mel-100-beta catalyst. The acid-catalysed reaction is suggested to occur via protonation of the benzaldehyde by the zeolitic protons and attack on the resulting cation by the enol form of the cyanoester. This nucleophilic reaction yields an alcohol, which can be dehydrated to form the ethyl *trans*-α-cyanocinnamate. Since the mel-20-beta catalyst has both protons and melaminium sites present, it is suggested that the reaction occurs via a combined mechanism as shown in scheme 6.

3.3. Catalyst comparisons

We observed that hydrotalcite effectively catalysed the Knoevenagel condensation of ethyl cyanoacetate and benzaldehyde with the conversion of 79.7% at 300 min. The results are shown in Fig. 7 for the first 300 min. It can be seen that these values are lower than those reported in the literature [25] which showed conversions of 31% and 88% after 15 min and 240 min, respectively. These values were found with an Mg/Al ratio of three at 60 °C with 5.5 wt% catalyst. As an increase in Al content results in a higher density of basic sites, it would be expected that the Mg/Al ratio of 2:1 and 80 °C would achieve higher conversions than the Mg/Al ratio of 3:1 at 60 °C. The layered structure of the hydrotalcite

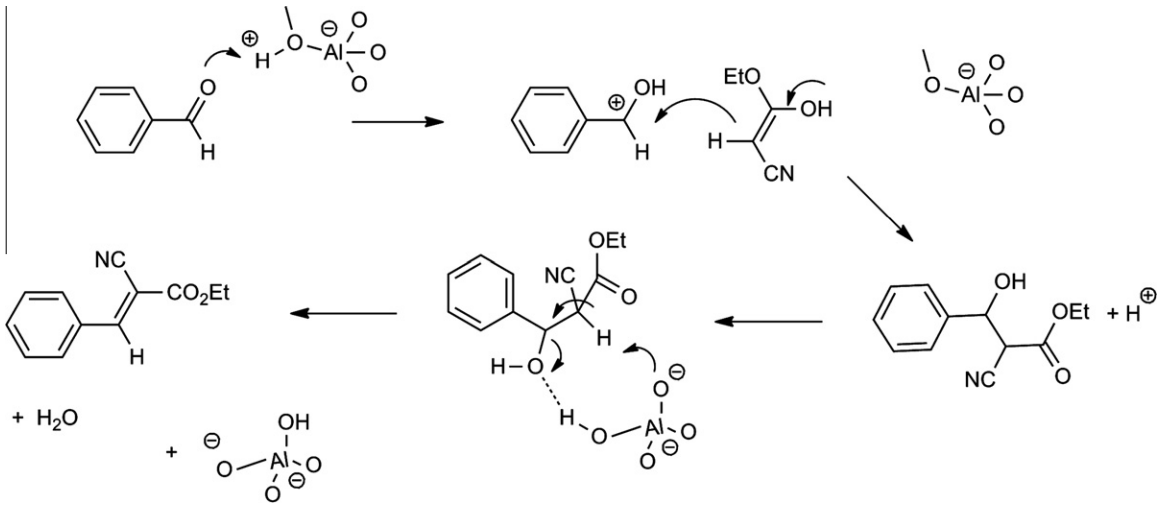

Scheme 4. Acid-catalysed condensation reaction (with H-beta zeolite catalyst).

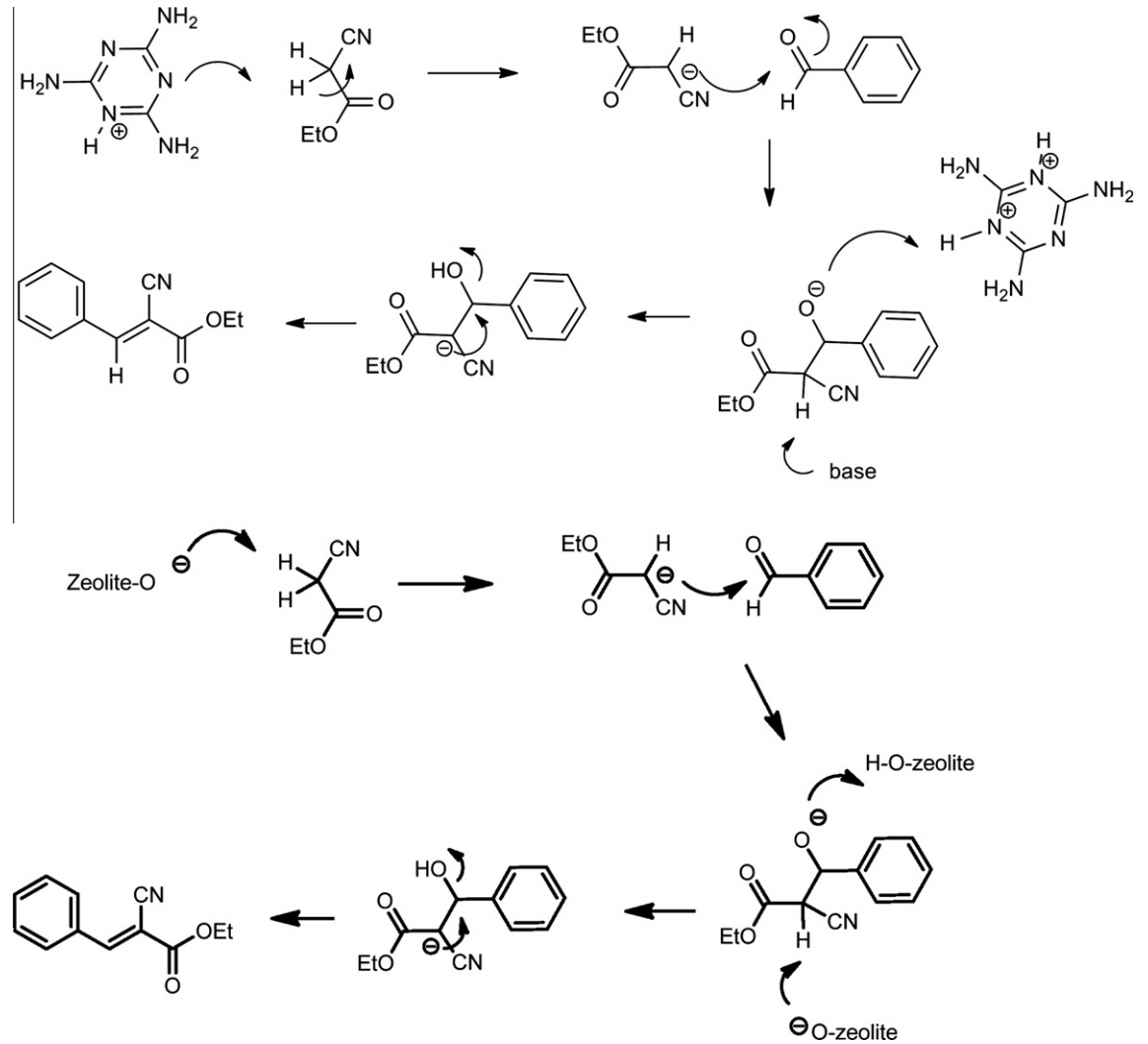

Scheme 5. Base-catalysed condensation reaction with mel-100-beta catalyst (above) and using the zeolite oxygen anion as the basic catalyst (below).

can explain the selectivity towards product formation, as no Michael addition product was seen.

Fig. 8 shows the result obtained for the MgO/Al_2O_3 catalyst. We observed product formation from using MgO/Al_2O_3 catalyst for the Knoevenagel condensation of ethyl cyanoacetate and benzaldehyde. Conversions of 63.2% and 99.8% were obtained after 300 and 1425 min, respectively.

The modification of MgO with Al_2O_3 creates a more basic catalyst, which would be expected to perform better than MgO due to an increased surface area. This idea is supported by a recent report

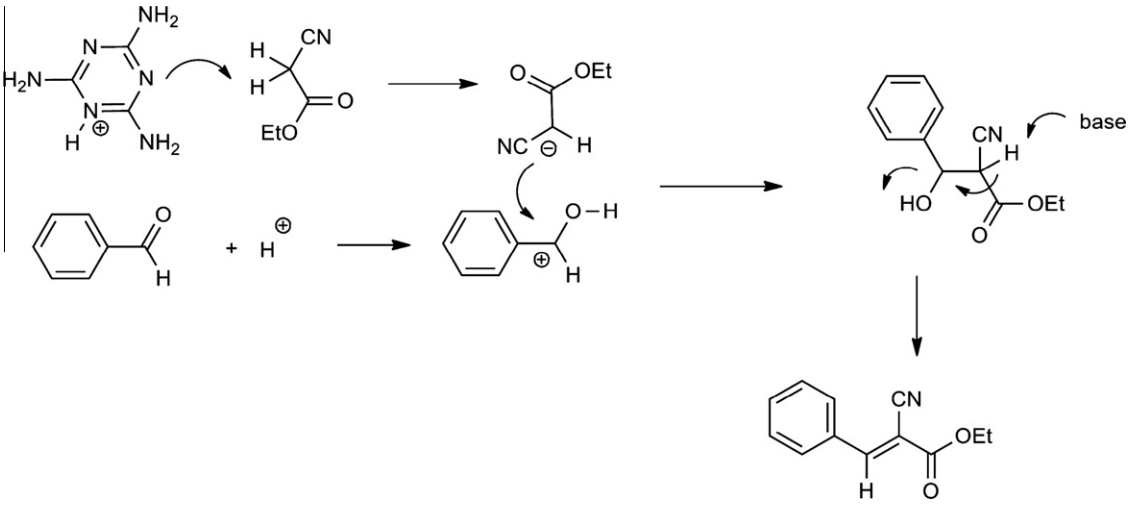

Scheme 6. Proposed mechanism for the synergistic relationship between the acidic and basic sites of the mel-20-beta zeolite catalyst.

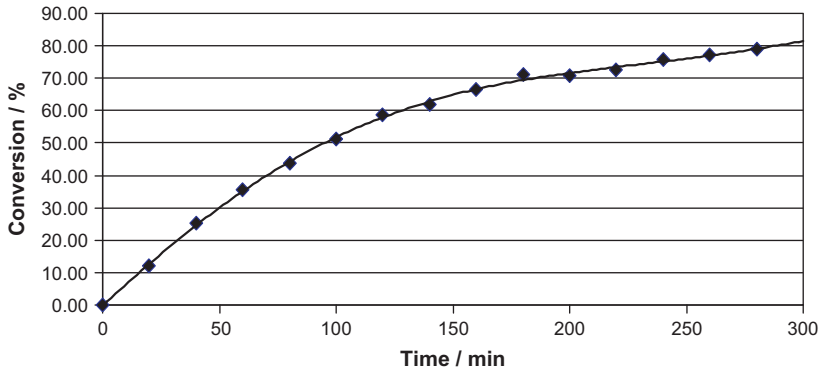

Fig. 7. Percentage conversion of ethyl cyanoacetate over the hydrotalcite catalyst as a function of time.

that showed a Mg–Sc–CO_3 catalyst displays stronger base sites and thus a higher activity resulting in greater conversions than Mg–Mn–CO_3 in the Knoevenagel condensation of ethyl cyanoacetate and benzaldehyde [12].

Fig. 9 shows a comparison for the three different catalysts over a period of 5 h, together with the blank run. It can be seen that the mel-20-beta hybrid zeolite catalyst performed the best after five hours with the order of reactivity, mel-20-beta > hydrotalcite > MgO/Al_2O_3 > un-catalysed. The same order was found for the initial reaction rates as can be observed from Fig. 9. It can be seen that the mel-20-beta zeolite has a significantly higher initial reaction rate which is over three times higher than the hydrotalcite. This suggests that the varying basicity of the catalysts plays a significant role in the kinetics of the reaction.

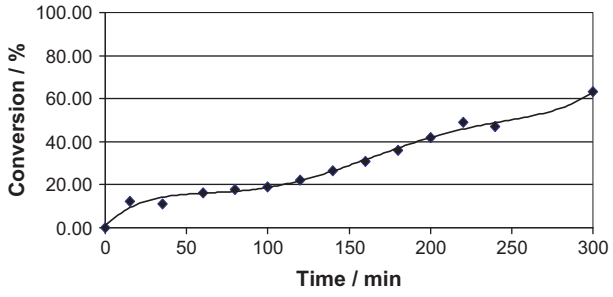

Fig. 8. Percentage conversion of ethyl cyanoacetate over MgO/Al_2O_3 as a function of time.

3.4. Variation of the mechanism depending on catalyst type

The different rates of reaction and end conversions of the Knoevenagel condensation suggest different reaction mechanisms for

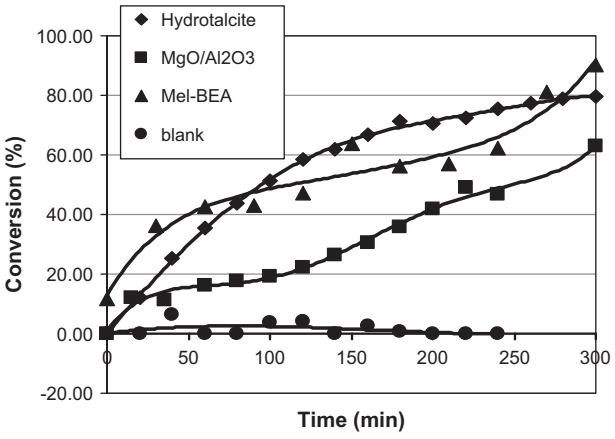

Fig. 9. Comparison of percentage conversion of ethyl cyanoacetate over hydrotalcite, MgO/Al_2O_3, the mel-20-beta zeolite catalyst and the blank as a function of time.

the formation of the ethyl *trans*-α-cyanocinnamate product. The observation of increased performance for not fully exchanged zeolite samples also suggests the necessity of some acid sites being present that enhance the catalytic performance of the newly developed catalysts. Schemes 4 and 5 illustrate proposed mechanisms that utilises acid (h-beta) and base (mel-100-beta) catalysts respectively. The possible role of the melaminium cation as a basic catalyst is shown in the upper part of Scheme 5. Although the medium of pK_b measurements are different to our reaction medium, it can be noted that melamine has a first pK_b of 9, and though the pK_b of its second protonation is not reported, a range of its deprotonated salts are easily prepared.

In our case (over mel-20-beta), a combination of these steps is speculated to be operating (Scheme 6). Active methylene groups upon deprotonation would react with the activated benzaldehyde, leading to the synthesis of the condensation product and a molecule of water. Indeed, a synergistic effect of acidic and basic sites has also been suggested for Aldol condensations over mesoporous materials with sulphonate and amine groups [14]. The sulphonate group in this case was suggested to aid the reaction via deprotonation–protonation of the acetone. This would be congruent with our results as zeolite beta in its acidic form produced poor conversions. Converting the majority of the acidic sites of the zeolite beta catalyst to basic sites using 100 mol% melamine based on aluminium content also produced a poor conversion. Besides a synergistic effect, the increased coverage could cause diffusion problems and thereby the converted products and the reactants would have greater difficulty exiting and entering the pore channels of the catalyst.

Using our data and literature, we can infer that a synergistic effect may be operational between the melamine base sites and the protonic acid sites. Scheme 6 outlines a likely mechanism, where the reaction between the deprotonated cyanoester and the protonated benzaldehyde ion is expected to increase the reactivity.

4. Conclusions

Simple modification of NH_4-beta zeolite with melamine leads to a catalyst containing extremely stable cationic melamine species in the cavities of the zeolite. This hybrid material is basic in nature. It exhibits good performance in the Knoevenagel condensation of benzaldehyde and ethyl cyanoacetate. The reaction rate, as well as the conversion of 93% was either comparable or significantly improved compared with other alkaline catalysts reported in the literature and to an acidic beta zeolite catalyst. We observed initial high rates that were higher than the initial reaction rates shown by the hydrotalcite and the MgO/Al_2O_3 catalysts. The activity in the condensation reaction is dependent on the amount and nature of acidic and basic sites present. The general stability of the catalyst shows potential for application to industrial scale reactions requiring mild basic and normally higher temperature conditions.

Acknowledgments

Financial support by Nottingham Trent University, UK and The University of Newcastle, Australia is gratefully acknowledged. The authors would like to thank Prof. B.Z. Dlugogorski, Prof. E.M. Kennedy and Prof. R.W. Joyner for useful discussions. We also acknowledge the use of CDS and the X-ray suite at UN and the Australian synchrotron and the SRS for the use of the facilities to determine aluminium EXAFS of the zeolite beta.

References

[1] S. Feast, J.A. Lercher, in: H. Chon, S.I. Woo, S.E. Park (Eds.), Recent Advances and New Horizons in Zeolite Science and Technology, Elsevier Science Publ. BV, Amsterdam, 1996, pp. 363–412.
[2] K. Tanabe, W.F. Holderich, Appl. Catal. A – Gen. 181 (1999) 399–434.
[3] Y. Okamoto, M. Ogawa, A. Maezawa, T. Imanaka, J. Catal. 112 (1988) 427–436.
[4] R.J. Davis, J. Catal. 216 (2003) 396–405.
[5] L.R.M. Martens, P.J. Grobet, P.A. Jacobs, Nature 315 (1985) 568–570.
[6] F. Winter, M. Wolters, A.J. van Dillen, K.P. de Jong, Appl. Catal. A – Gen. 307 (2006) 231–238.
[7] H. Mei, M. Hu, H.X. Ma, H.Q. Yao, J. Shen, Fuel Process. Technol. 88 (2007) 343–348.
[8] J.H. Kwak, J. Szanyi, C.H.F. Peden, Catal. Today 89 (2004) 135–141.
[9] T. Seki, M. Onaka, J. Mol. Catal. A – Chem. 263 (2007) 115–120.
[10] A. Derrien, G. Renard, D. Brunel, Mesoporous Mol. Sieves (1998) 445–452.
[11] S. Jaenicke, G.K. Chuah, X.H. Lin, X.C. Hu, Microporous Mesoporous Mater. 35–36 (2000) 143–153.
[12] X.H. Lin, G.K. Chuah, S. Jaenicke, J. Mol. Catal. A – Chem. 150 (1999) 287–294.
[13] B.M. Choudary, M.L. Kantam, P. Sreekanth, T. Bandopadhyay, F. Figueras, A. Tuel, J. Mol. Catal. A – Chem. 142 (1999) 361–365.
[14] K. Narasimharao, M. Hartmann, H.H. Thiel, S. Ernst, Microporous Mesoporous Mater. 90 (2006) 377–383.
[15] J. Zhou, Z. Hua, J. Zhao, Z. Gao, S.Z. Zeng, J.L. Shi, J. Mater. Chem. 20 (2010) 6764–6771.
[16] L. Martins, D. Cardoso, Microporous Mesoporous Mater. 106 (2007) 8–16.
[17] M.J. Climent, A. Corma, S. Iborra, A. Velty, J. Mol. Catal. A – Chem. 182 (2002) 327–342.
[18] R.K. Zeidan, M.E. Davis, J. Catal. 247 (2007) 379–382.
[19] A. Corma, V. Fornes, R.M. Martinaranda, H. Garcia, J. Primo, Appl. Catal. 59 (1990) 237–248.
[20] L. Costa, G. Camino, J. Thermal Anal. Calorimetry 34 (1988) 423–429.
[21] CIPCS, Melamine, International Programme on Chemical Safety, 2005.
[22] S. Chen, Y. Yang, K. Zhang, J. Wang, Catal. Today 116 (2006) 2–5.
[23] J.M. Newsam, M.M.J. Treacy, W.T. Koetsier, C.B.D. Gruyter, Proc. Roy. Soc. Lond. A Math. Phys. Sci. 420 (1988) 375–405.
[24] M.M.J. Treacy, J.M. Newsam, Nature 332 (1988) 249–251.
[25] A. Hayashi, H. Nakayama, M. Tsuhako, Solid State Sci. 11 (2009) 1007–1015.
[26] M.L.M. Bonati, R.W. Joyner, M. Stockenhuber, Microporous Mesoporous Mater. 104 (2007) 217–224.
[27] L. Martins, K.M. Vieira, L.M. Rios, D. Cardoso, Catal. Today 133-135 (2008) 706–710.
[28] L. Martins, W. Hoelderich, D. Cardoso, J. Catal. 258 (2008) 14–24.
[29] T. Hasegawa, C.K. Krishnan, M. Ogura, Microporous Mesoporous Mater. 132 (2010) 290–295.
[30] F.H. Allen, Acta Crystallogr. Sect. B – Struct. Sci. 58 (2002) 380–388.
[31] H.P. Jing, M. Strobele, M. Weisser, H.J. Meyer, Zeitschrift Fur Anorganische Und Allgemeine Chemie 629 (2003) 368–370.
[32] J. Janczak, G.J. Perpetuo, Acta Crystallogr. Sect. C – Crystal Struct. Commun. 57 (2001) 1431–1433.
[33] K. Wijaya, O. Moers, D. Henschel, A. Blaschette, P.G. Jones, Zeitschrift Fur Naturforschung (Section B – A J. Chem. Sci.) 59 (2004) 747–756.
[34] G.J. Perpetuo, J. Janczak, Acta Crystallogr. Sect. C – Crystal Struct. Commun. 62 (2006) O372–O375.
[35] A. Heine, K. Gloe, T. Doert, Zeitschrift Fur Anorganische Und Allgemeine Chemie 634 (2008) 452–456.
[36] A. Martin, A.A. Pinkerton, Acta Crystallogr. Sect. C – Crystal Struct. Commun. 51 (1995) 2174–2177.
[37] R.V. Siriwardane, M.S. Shen, E.P. Fisher, Energy Fuels 19 (2005) 1153–1159.
[38] M. Stockenhuber, J.A. Lercher, Microporous Mater. 3 (1995) 457–465.
[39] J. Howard, P.J. Lux, J. Yarwood, Zeolites 8 (1988) 427–431.
[40] S. Akyuz, T. Akyuz, J. Incl. Phenom. Macrocyc. Chem. 48 (2004) 75–80.
[41] S. Saravanamurugan, M. Palanichamy, M. Hartmann, V. Murugesan, Appl. Catal. A – Gen. 298 (2006) 8–15.
[42] R.W. Joyner, A.D. Smith, M. Stockenhuber, M.W.E. van den Berg, Phys. Chem. Chem. Phys. 6 (2004) 5435–5439.
[43] A.B. Wiles, D. Bozzuto, C.L. Cahill, R.D. Pike, Polyhedron 25 (2006) 776–782.
[44] C.J. Pouchert, The Aldrich Library of Infrared Spectra. Aldrich Chemical Company, Milwaukee, WI, 1997, 5100.
[45] D. Lin-Vien, N.B. Colthup, W.G. Fateley, J.G. Graselli, The Handbook of Infrared and Raman Characteristic Frequencies of Organic Molecules, Academic Press, San Diego, CA, 1991. 503.
[46] J. Pironon, M. Pelletier, P. de Donato, R. Mosser-Ruck, Clay Minerals 38 (2003) 201–211.
[47] X.F. Zhang, E.S.M. Lai, R. Martin-Aranda, K.L. Yeung, Appl. Catal. A – Gen. 261 (2004) 109–118.
[48] K. Komura, T. Kawamura, Y. Sugi, Catal. Commun. 8 (2007) 644–648.